

Predicting the Charge Density Response in Metal Electrodes

Andrea Grisafi,^{1,*} Augustin Bussy,² Mathieu Salanne,^{3,4} and Rodolphe Vuilleumier¹

¹*PASTEUR, Département de chimie, École Normale Supérieure,
PSL University, Sorbonne Université, CNRS, 75005 Paris, France*

²*Department of Chemistry, University of Zurich,
Winterthurerstrasse 190, 8057 Zürich, Switzerland*

³*Sorbonne Université, CNRS, Physicochimie des Électrolytes et Nanosystèmes Interfaciaux, F-75005 Paris, France*

⁴*Institut Universitaire de France (IUF), 75231 Paris, France*

The computational study of energy storage and conversion processes calls for simulation techniques that can reproduce the electronic response of metal electrodes under electric fields. Despite recent advancements in machine-learning methods applied to electronic-structure properties, predicting the non-local behavior of the charge density in electronic conductors remains a major open challenge. We combine long-range and equivariant kernel methods to predict the Kohn-Sham electron density of metal electrodes in response to various kinds of electric field perturbations. By taking slabs of gold as an example, we first show how the non-local electronic polarization generated by the interaction with an ionic species can be accurately reproduced in electrodes of arbitrary thickness. A finite-field extension of the method is then introduced, which allows us to predict the charge transfer and the electrostatic potential drop induced by the application of a homogeneous and constant electric field. Finally, we demonstrate the capability of the method to reproduce the charge-density response in a gold/electrolyte capacitor under an applied voltage, predicting the system polarization with a greater accuracy than state-of-the-art classical atomic-charge models.

The behaviour of the electronic charge density in metal surfaces plays a decisive role in the study of energy storage and conversion processes occurring in batteries, capacitors and electrocatalytic frameworks [1–3]. Its accurate computer simulation ultimately requires the adoption of first-principles methods that are capable to predict the non-local response of an electronic conductor subject to an external perturbation. Density functional theory (DFT), in particular, has been widely applied to the description of metal interfaces in various research areas of surface chemistry and catalysis [4–6]. Depending on the specific application, different methods can be adopted to keep the metal at a constant charge [7, 8], fixed applied potential [9–14], as well as to induce a macroscopic polarization in the system due to the presence of an applied field [15–17]. In spite of the success of these approaches, the extensive use of DFT to the study of realistic metal interfaces is however hindered by an unfavorable scaling with the system size, effectively limiting their applicability to a few hundreds of atoms [18, 19].

Beyond first-principles approaches, classical molecular dynamics (MD) methods have also gained major attention in the context of enabling the simulation of metal interfaces at the nanometric scale [20]. These methods go from the adoption of fluctuating atomic charges [21–25] to the use of image-charge boundary conditions [26, 27]. The downside of MD is of course the lack of an explicit quantum treatment, which limits the description of the electrode either to a perfect metal approximation, or to the adoption of a finite screening length computed from semiclassical Thomas-Fermi models [28, 29]. For these reasons, reaching the level of accuracy of DFT in the large-scale simulation of the metal charge density represents a goal of paramount importance [30, 31].

In recent years, many efforts have been devoted to the development of machine-learning (ML) methods dedicated to the prediction of the electronic charge density [32–41]. The success of these methods is mostly grounded on the interplay between a local decomposition of the scalar field and the adoption of local representations of the atomic structure that are used as input vectors of the ML model. When it comes to conducting systems, however, local ML models are expected to show strong limitations in predicting the variations of the charge density over large distances, especially in the presence of external fields. In fact, while some ML methods that explicitly incorporate long-range effects have already been developed [42–45], the study of charge-transfer phenomena in electronic conductors has to date been limited to simplified charge-equilibration schemes that represent the electron density via a set of atomic charges [46–48]. Moreover, an explicit ML-treatment of the charge density in metal surfaces under electric fields has thus far only been investigated by virtue of suitable response functions that enter conceptual DFT approaches [49, 50]. In this letter, we show how to combine long-range and equivariant learning methods to accurately predict the charge density response in metal electrodes, including the derivation of a finite-field model suitable to treat the application of external electric fields.

Let us start by considering the linear expansion of the electron density on an atom-centered basis $\chi_{n\lambda\mu}$ given by the product of radial Gaussian-type functions R_n^λ and spherical harmonics $Y_{\lambda\mu}$:

$$n_e(\mathbf{r}) \approx \sum_{in\lambda\mu} c_i^{n\lambda\mu} \sum_{ix,iy} \chi_{n\lambda\mu}(\mathbf{r} - \mathbf{r}_i - \mathbf{u}_{ix,iy}), \quad (1)$$

where \mathbf{r}_i are the atomic positions in the unit cell and $\mathbf{u}_{ix,iy}$ are the cell translation vectors used to account for

the two dimensional periodicity of the metallic surface. We assume that the coefficients $c_i^{n\lambda\mu}$ come from a density-fitting procedure of a reference Kohn-Sham density.

The decomposition of Eq. (1) can be used within equivariant ML models to predict n_e in a highly transferable (atom-centered) fashion [35, 41]. In this work, we rely on a recently optimized kernel-based method introduced in Ref. [40], also known as SALTED. Within SALTED, a linear approximation of the density expansion coefficients is provided which satisfies the rotational symmetry of spherical harmonics, i.e., $\mathbf{c}_i^{n\lambda} = \sum_M \mathbf{k}_{iM}^\lambda \mathbf{b}_M^{n\lambda}$. Here, $\mathbf{b}_M^{n\lambda}$ are vector-valued regression weights of dimension $(2\lambda + 1)$ and \mathbf{k}_{iM}^λ is a symmetry-adapted kernel matrix of dimension $(2\lambda + 1)^{\otimes 2}$ which encodes the similarity between the local structural features of atom i and those of a sparse selection of atoms $\{M\}$ belonging to the training set [51]. The complexity of the learning problem then comes down to the adoption of physically inspired structural representations of the atomic environment [52], \mathbf{P}_i^λ , which define the kernel matrix as an inner product over a suitable feature space [53], i.e., $\mathbf{k}_{iM}^\lambda = \mathbf{P}_i^\lambda \mathbf{P}_M^{\lambda\dagger}$.

A typical choice for \mathbf{P}_i^λ consists in an equivariant generalization of the popular smooth overlap of atomic positions (SOAP) method [51, 54]. This approach ultimately derives from the definition of a smooth Gaussian-density distribution describing the local environment of atom i , i.e., $\rho_i(\mathbf{r}) = f_{\text{cut}}(r) \sum_j e^{-\alpha|\mathbf{r}-\mathbf{r}_{ij}|^2}$, with j running over the atomic neighbours and $f_{\text{cut}}(r)$ a spherical cutoff function of radius r_{cut} . By construction, the model thus neglects any long-range effect that occurs beyond r_{cut} in exchange of a high level of transferability. While this is generally not a problem [39, 55], we aim to demonstrate that endowing the structural features with a long-range character is essential when dealing with metal surfaces. For this reason, we rely on a definition of \mathbf{P}_i^λ based on long-distance equivariant (LODE) representations [56]. In particular, we adopt an implementation of LODE that combines information about the local atomic density $\rho_i(\mathbf{r})$ and a Hartree-like potential originated by the Gaussian density of the atoms of the entire system [57]:

$$V_i(\mathbf{r}) = f_{\text{cut}}(r) \int d\mathbf{r}' \frac{\sum_j e^{-\alpha|\mathbf{r}'-\mathbf{r}_{ij}|^2}}{|\mathbf{r}'-\mathbf{r}|}. \quad (2)$$

Note that the cutoff function is here applied *after* the Coulomb operator, thus guaranteeing the inclusion of long-range information within the local environment of i . The descriptor of order λ is finally obtained from a symmetry-adapted tensor product of ρ_i and V_i expanded on a set of orthogonal radial and angular functions [57, 58]:

$$P_i^{\lambda\mu}(nn'll') = \sum_{mm'} \rho_i^{n\lambda m} V_i^{n'l'm'} \langle lm, l'm' | \lambda\mu \rangle, \quad (3)$$

where n and lm are the radial and angular indexes, respectively, and where $\langle lm, l'm' | \lambda\mu \rangle$ are the Clebsch-Gordan coefficients used for the composition of angular momenta.

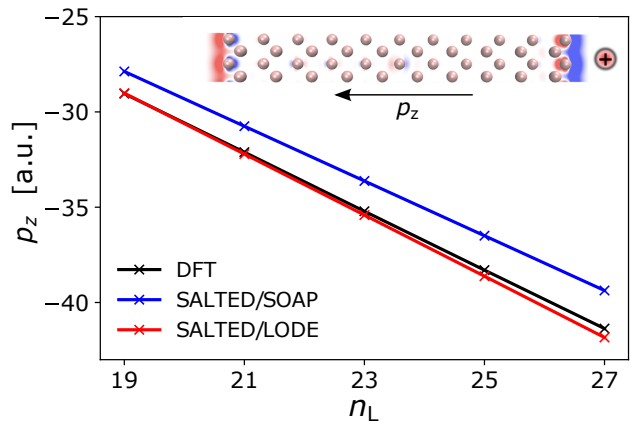


FIG. 1. Extrapolated electronic polarization p_z of Au(100) electrodes of increasing thickness n_L , induced by a Na^+ cation placed at 4 Å distance from the upper metal surface. Predictions are obtained for SALTED/SOAP (blue line) and SALTED/LODE (red line) models trained on the electron-density response of electrodes that include up to $n_L=15$ atomic layers. Black line: reference DFT polarization. Inset: volume slice of the predicted charge density response for a $n_L=21$ gold electrode; color code from blue to red corresponds to a linear scale from -0.001 to $+0.001$ a.u., respectively.

We start by considering slabs of gold aligned perpendicularly to the z -axis, which interact with a sodium cation Na^+ placed at 4 Å distance from the upper metal surface. In particular, we consider symmetric Au(100) slabs made of 2 unit cell repetitions along the xy plane and spanning from 3 to 15 gold layers along z . A total of 240 training configurations are then generated by taking uniform random displacements of the atomic positions up to 2.5% of the lattice constant along the three Cartesian directions. The electrode polarization is simulated at the QM/MM level of theory by representing the ion as a classical Gaussian charge [59]. Reference density coefficients $c_i^{n\lambda\mu}$ for the gold electrodes are obtained by performing calculations of n_e at the DFT/PBE level [60], in combination with a density-fitting approach based on an overlap metric [61–63]. The learning target is finally defined as the difference between the perturbed electron densities and the electron densities of the corresponding isolated electrodes, i.e., $\Delta n_e = n_e - n_e^0$.

From a ML point of view, the ion-induced polarization of the metal electrode is expected to be naturally captured by a multispecies treatment of Eq. (3). This accounts for computing as many ρ_i and V_i as the number of chemical species a in the system [57, 64], while letting i run exclusively on the gold atoms. Upon this procedure, we train SALTED/LODE models using a local cutoff of $r_{\text{cut}} = 8\text{Å}$, where the atom density and potential fields are defined from Gaussian widths of $\sigma = 0.5\text{Å}$ and $\sigma = 4.0\text{Å}$, respectively. For comparison, SALTED/SOAP models are similarly trained by substituting V_i with ρ_i in Eq. (3). Further details about the reference calcula-

tions and machine-learning parameters are reported in the Supplemental Material (SM), Ref. [65].

We put the method to the test on rigid gold electrodes that include from $n_L=19$ to $n_L=27$ atomic layers. In so doing, we extrapolate the charge-density response over a range of distances between the two metal surfaces that extends well beyond that spanned by the training set. As an accuracy measure of the ion-induced charge transfer, we compute the metal electronic polarization along z , p_z , which can be analytically obtained from the predicted density coefficients [65]. Fig. 1 reports the prediction results as a function of the number of atomic layers n_L . As expected, we find that a local SOAP-based model is unable to reproduce the long-range character of the charge-density response, resulting in predicted polarization values that are off by $\sim 36\%$ of the standard deviation of p_z in the test set. Conversely, SALTED/LODE predictions are found to accurately extrapolate the electronic polarization at increasing electrode thicknesses, thus capturing the expected linear decrease of p_z with respect to n_L . This is confirmed by the density-derived calculation of the Hartree potential drop through the metallic slab, which is found in very good agreement with that of DFT for all the test electrodes considered [65]. We note that performing these predictions took ~ 1 second per structure on a single node with 24 CPUs, resulting in a speedup of the order of 3×10^3 with respect to DFT [65].

Having shown the importance of long-range structural information in describing the response properties of metal electrodes, we now proceed with investigating the charge transfer effect induced by an applied electric field. From here on, we will only refer to SALTED/LODE models. The accumulation/depletion of electronic charge at the two metal surfaces is simulated by performing calculations under a constant and uniform electric field along z . The field intensity is chosen as $E_z = -1.0$ V/Å, which, for a perfect metal, corresponds to an induced surface charge of $\sigma = \pm 5.53 \times 10^{-3}$ e/Å². DFT densities are generated from the same gold configurations and using the same level of theory already adopted in the previous example.

In order to reproduce the polarization of the electrode induced by an applied electric field E_z , the axial symmetry of the system around z must be explicitly incorporated into the ML model. To tackle this problem, we start by defining a local external potential field centered at the position of a given atom i :

$$V_i^E(\mathbf{r}) = E_z(z - z_i)f_{\text{cut}}(r). \quad (4)$$

An equivariant descriptor $\mathbf{P}_i^{\lambda,E}$ that automatically satisfies the symmetry of the applied field can then be directly obtained by substituting V_i with V_i^E in Eq. (3). Specifically, we find that the field symmetry is manifested in the selection rules $l = \lambda \pm 1$ and $m = \mu$ [65]. A ML representation of n_e able to reproduce the non-local charge-density response can be finally constructed via a suitable coupling

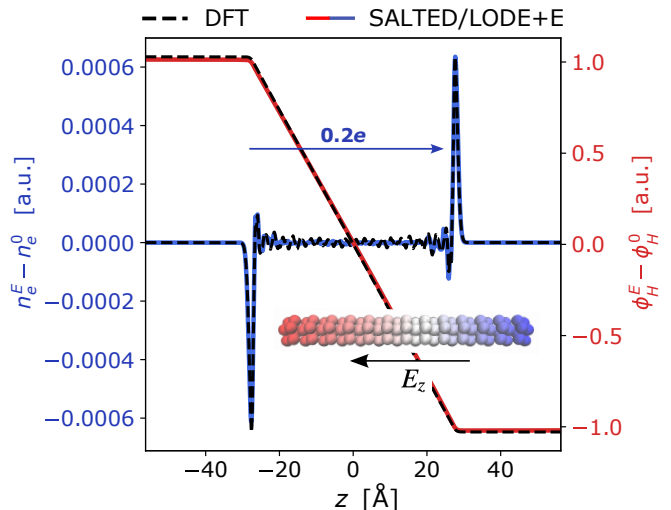


FIG. 2. Extrapolated density and potential response averaged over the xy plane of a Au(100) electrode with 27 metal layers under an applied electric field $E_z = -1$ V/Å. Blue line: electron density response. Red line: Hartree potential response. Black dashed line: reference DFT response. Predictions are obtained from a field-dependent SALTED/LODE+E model trained on a dataset which includes electrodes with $n_L^{\text{max}}=15$. Inset: representation of the predicted $\phi_H^E - \phi_H^0$ through the metal electrode; color code from blue to red corresponds to a linear scale from -1.0 to $+1.0$ a.u., respectively.

between $\mathbf{P}_i^{\lambda,E}$ and the LODE descriptor of Eq. (3):

$$\tilde{\mathbf{P}}_i^{\lambda,E} \equiv \left(\mathbf{P}_i^\lambda \oplus \mathbf{P}_i^{\lambda,E} \right) \otimes \mathbf{P}_i^0. \quad (5)$$

Note that these algebraic operations account for taking simple sums and products of the individual kernels, thus keeping the dimensionality of the learning problem unchanged with respect to the no-field case (kernel trick [66]). A detailed derivation is reported in the SM [65].

To test the capability of the previously discussed model to predict the electronic charge transfer induced by the applied electric field, we now repeat the size extrapolation exercise already carried out in the previous example, so that the same training and test gold structures are used. Fig. 2 reports the predicted charge-density response for the largest test electrode considered, as compared with the corresponding DFT profile. In spite of the highly extrapolative regime, our finite-field extension of LODE allows us to accurately reproduce the accumulation/depletion of opposite electronic charge at the two sides of the metal electrode, predicting a charge transfer of $0.2e$ that is in perfect agreement with that of DFT. To corroborate these results, we report in the same Figure the variation of the Hartree potential, $\Delta\phi_H$, which can be directly computed from the predicted Δn_e [65]. We find that the expected potential drop of ~ 2 a.u. between the two metal surfaces is accurately predicted, reproducing the linear decrease of $\Delta\phi_H$ in the metallic bulk in order to perfectly screen the opposite increase of the external potential $\phi_{\text{ext}} = -E_z z$.

We continue by showcasing an example where a rigid Au(100) electrode made of 4 unit cell repetitions along the xy plane and 7 metal layers is put in contact with a concentrated water/NaCl solution under a uniform electric field E_z , Fig. 3-a). Following Ref. [67], a similar setup can be used with 3D periodic boundary conditions to simulate an ionic capacitor under an applied voltage $\Delta V = -E_z L_z$, with L_z the length of the simulation box. In this example, an electric field $E_z = 0.016$ V/Å is applied to represent an ionic capacitor subject to a potential difference of $\Delta V = -1.0$ V. To generate electrolyte configurations that are representative of the given ensemble at $T = 298$ K, we run finite- E classical molecular dynamics [68] over 10 ns, using the MetalWalls simulation program [69]. From the trajectory so generated, QM/MM calculations of the electrode charge density under the applied electric field E_z are then performed for 2000 uncorrelated configurations. In particular, we treat the gold slab at the same DFT level of theory already adopted in the previous examples, while representing the aqueous electrolyte via classical Gaussian charges [59]. Note that because of the classical nature of the electrolyte, setting the electrode in the middle of the simulation box is enough to avoid problems related to the discontinuous jump of the external potential at $z = L_z$. The difference between the QM/MM density and the density of the isolated electrode under E_z is finally considered as a learning target of the SALTED problem.

We select 1600 random configurations for training and retain the remaining 400 for testing. SALTED/LODE models are constructed from atom density and potential fields defined from Gaussian widths of $\sigma = 0.5$ Å and $\sigma = 1.0$ Å, respectively, which are both cut off at $r_{\text{cut}} = 10$ Å. Fig. 3-b) reports the ML predictions of the derived electrode polarization p_z against the reference DFT values. In so doing, we also compare results obtained from the classical MetalWalls simulation. We observe that MetalWalls yields a systematic overestimation of the electrode polarization, which accounts for an average deviation of $\langle \Delta p_z \rangle = 1.2$ a.u. with respect to DFT. Conversely, our SALTED/LODE model is able to accurately reproduce the charge-density response induced by the field of the various electrolyte configurations. In particular, the derived ML predictions of p_z present a small root mean square error of 2.9% of the standard deviation of the polarization vector in the test set. This is in line with the excellent agreement between the DFT and predicted response averaged over the xy -plane, $\Delta \bar{n}_e(z)$, as reported in the inset of the Figure for a representative test configuration. Performing similar predictions took, on average, ~ 5 seconds per structure on 128 CPUs versus ~ 5 minutes of DFT. A substantial speedup of the ML performance will be achieved in the future by relying on a particle mesh Ewald implementation of the LODE potential [70].

We conclude by providing an estimate of the electrical double-layer (EDL) contribution to the differential capacitance of the system, defined from the electrolyte-induced

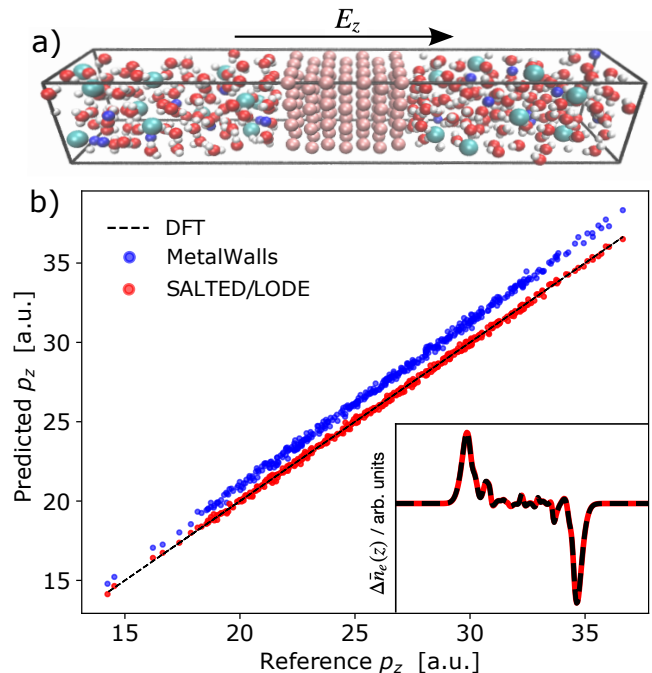


FIG. 3. a) Representation of the physical system under study: a gold electrode is put in contact with a water/NaCl solution under an applied electric field $E_z = 0.016$ V/Å, corresponding to a potential drop of -1.0 V through the simulation cell [67]. b) Electrode polarization p_z as predicted from the electron-density response induced by 400 electrolyte configurations. Predictions are reported against the reference QM/MM values. Black dashed line: DFT. Blue dots: classical MetalWalls result [69]. Red dots: SALTED/LODE results. Inset: predicted electron-density response averaged over the xy -plane for a representative electrode/electrolyte configuration (red line), as compared with the reference DFT profile.

fluctuations of the integrated charge $\pm Q$ accumulated at the two metal surfaces, i.e., $C_{\text{diff}}^{\text{EDL}} = \beta \langle \delta Q^2 \rangle$ [25]. Similarly to the case of p_z , the calculation of Q can be performed analytically from the isotropic charge-density components [65]. Upon predicting Q for 5500 uncorrelated frames of a MetalWalls trajectory of 30ns, we obtain $C_{\text{diff}}^{\text{EDL}} = 8.9$ $\mu\text{F}/\text{cm}^2$. This value is sensibly smaller than what can be obtained from the classical MetalWalls simulation, i.e., $C_{\text{diff}}^{\text{EDL}} = 10.5$ $\mu\text{F}/\text{cm}^2$, which is found to give larger fluctuations of the electrode surface charge with respect to the corresponding ML predictions [65]. By and large, these results highlight the importance of going beyond a classical picture when describing non-local polarization effects in finite conducting materials.

The presented study shows how the interplay of equivariant, long-range and finite-field learning models can be used to accurately predict the quantum-mechanical response of metal electrodes under electric fields of different nature. In perspective, the ready access to the charge-density response can provide a rigorous pathway to accurately compute the polarization energy of generic

electrochemical interfaces, while having the permanent electrostatics accurately incorporated via local ML models of the electron density [39]. In this context, an application of major impact will consist in driving the long-range dynamics of the system at a ML/MM level of theory [30]. Finally, we foresee applications of the method in determining the capability of the metal surface to undergo electron-transfer processes [71], as well in predicting optical response functions [72] that can serve for a spectroscopic characterization of the interface [73].

The authors are grateful to Ari Paavo Seitsonen, Federico Grasselli and Kevin Rossi for useful discussion. AG acknowledges funding from the Swiss National Science Foundation, Grant No. P2ELP2-199747. This work was supported by the French National Research Agency under the France 2030 program (Grant ANR-22-PEBA-0002). Simulations of the ionic capacitor were performed on the Luxembourg national supercomputer MeluXina (Grant EHPC-REG-2022R02-244).

* andrea.grisafi@ens.psl.eu

- [1] A. K. Lautar, J. Bitenc, T. Rejec, R. Dominko, J.-S. Filhol, and M.-L. Doublet, *Journal of the American Chemical Society* **142**, 5146 (2020).
- [2] S. D. Beinlich, N. G. Hörmann, and K. Reuter, *ACS Catalysis* **12**, 6143 (2022).
- [3] N. Karmodak, L. Bursi, and O. Andreussi, *The Journal of Physical Chemistry Letters* **13**, 58 (2022).
- [4] J. K. Nørskov, F. Abild-Pedersen, F. Studt, and T. Bligaard, *Proceedings of the National Academy of Sciences* **108**, 937 (2011).
- [5] B. Grosjean, M.-L. Bocquet, and R. Vuilleumier, *Nature Communications* **10**, 1656 (2019).
- [6] N. Gerrits, E. W. F. Smeets, S. Vuckovic, A. D. Powell, K. Doblhoff-Dier, and G.-J. Kroes, *The Journal of Physical Chemistry Letters* **11**, 10552 (2020).
- [7] A. M. Souza, I. Rungger, C. D. Pemmaraju, U. Schwingenschloegl, and S. Sanvito, *Phys. Rev. B* **88**, 165112 (2013).
- [8] C. Freysoldt, A. Mishra, M. Ashton, and J. Neugebauer, *Phys. Rev. B* **102**, 045403 (2020).
- [9] A. Y. Lozovoi, A. Alavi, J. Kohanoff, and R. M. Lynden-Bell, *The Journal of Chemical Physics* **115**, 1661 (2001).
- [10] J.-S. Filhol and M. Neurock, *Angewandte Chemie International Edition* **45**, 402 (2006).
- [11] K. Letchworth-Weaver and T. A. Arias, *Phys. Rev. B* **86**, 075140 (2012).
- [12] N. G. Hörmann, O. Andreussi, and N. Marzari, *The Journal of Chemical Physics* **150**, 041730 (2019).
- [13] M. M. Melander, M. J. Kuisma, T. E. K. Christensen, and K. Honkala, *The Journal of Chemical Physics* **150**, 041706 (2019).
- [14] F. Domínguez-Flores and M. M. Melander, *The Journal of Chemical Physics* **158**, 144701 (2023).
- [15] M. Stengel and N. A. Spaldin, *Phys. Rev. B* **75**, 205121 (2007).
- [16] F. Che, J. T. Gray, S. Ha, and J.-S. McEwen, *ACS Catalysis* **7**, 551 (2017).
- [17] C. Ke, Z. Lin, and S. Liu, *ACS Catalysis* **12**, 13542 (2022).
- [18] R. Khatib, A. Kumar, S. Sanvito, M. Sulpizi, and C. S. Cucinotta, *Electrochimica Acta* **391**, 138875 (2021).
- [19] A. Chen, J.-B. Le, Y. Kuang, and J. Cheng, *The Journal of Chemical Physics* **157**, 094702 (2022).
- [20] G. Jeanmairet, B. Rotenberg, and M. Salanne, *Chemical Reviews* **122**, 10860 (2022).
- [21] J. I. Siepmann and M. Sprik, *The Journal of Chemical Physics* **102**, 511 (1995).
- [22] S. K. Reed, O. J. Lanning, and P. A. Madden, *The Journal of Chemical Physics* **126**, 084704 (2007).
- [23] S. K. Reed, P. A. Madden, and A. Papadopoulos, *The Journal of Chemical Physics* **128**, 124701 (2008).
- [24] D. T. Limmer, C. Merlet, M. Salanne, D. Chandler, P. A. Madden, R. van Roij, and B. Rotenberg, *Phys. Rev. Lett.* **111**, 106102 (2013).
- [25] L. Scalfi, D. T. Limmer, A. Coretti, S. Bonella, P. A. Madden, M. Salanne, and B. Rotenberg, *Phys. Chem. Chem. Phys.* **22**, 10480 (2020).
- [26] M. K. Petersen, R. Kumar, H. S. White, and G. A. Voth, *The Journal of Physical Chemistry C* **116**, 4903 (2012).
- [27] K. A. Dwelle and A. P. Willard, *The Journal of Physical Chemistry C* **123**, 24095 (2019).
- [28] L. Scalfi, T. Dufils, K. G. Reeves, B. Rotenberg, and M. Salanne, *The Journal of Chemical Physics* **153**, 174704 (2020).
- [29] L. Scalfi and B. Rotenberg, *Proceedings of the National Academy of Sciences* **118**, e2108769118 (2021).
- [30] N. Di Pasquale, J. D. Elliott, P. Hadjidoukas, and P. Carbone, *Journal of Chemical Theory and Computation* **17**, 4477 (2021).
- [31] N. Di Pasquale, A. R. Finney, J. D. Elliott, P. Carbone, and M. Salvalaglio, *The Journal of Chemical Physics* **158**, 134714 (2023).
- [32] F. Brockherde, L. Vogt, L. Li, M. E. Tuckerman, K. Burke, and K. R. Müller, *Nat. Commun.* **8**, 872 (2017).
- [33] J. M. Alred, K. V. Bets, Y. Xie, and B. I. Yakobson, *Composites Science and Technology* **166**, 3 (2018).
- [34] A. Chandrasekaran, D. Kamal, R. Batra, C. Kim, L. Chen, and R. Ramprasad, *npj Comput Mater* **5**, 22 (2019).
- [35] A. Grisafi, A. Fabrizio, B. Meyer, D. M. Wilkins, C. Corminboeuf, and M. Ceriotti, *ACS Cent. Sci.* **5**, 57 (2019).
- [36] A. Fabrizio, A. Grisafi, B. Meyer, M. Ceriotti, and C. Corminboeuf, *Chem. Sci.* **10**, 9424 (2019).
- [37] M. Bogojeski, L. Vogt-Maranto, M. E. Tuckerman, K.-R. Müller, and K. Burke, *Nat. Commun.* **11**, 5223 (2020).
- [38] P. B. Jørgensen and A. Bhowmik, *npj Computational Materials* **8**, 183 (2022).
- [39] A. M. Lewis, A. Grisafi, M. Ceriotti, and M. Rossi, *Journal of Chemical Theory and Computation* **17**, 7203 (2021).
- [40] A. Grisafi, A. M. Lewis, M. Rossi, and M. Ceriotti, *Journal of Chemical Theory and Computation* **19**, 4451 (2023).
- [41] J. A. Rackers, L. Tecot, M. Geiger, and T. E. Smidt, *Machine Learning: Science and Technology* **4**, 015027 (2023).
- [42] A. Grisafi and M. Ceriotti, *The Journal of Chemical Physics* **151**, 204105 (2019).
- [43] A. Gao and R. C. Remsing, *Nature Communications* **13**, 1572 (2022).
- [44] L. Zhang, H. Wang, M. C. Muniz, A. Z. Panagiotopoulos,

- R. Car, and W. E, The Journal of Chemical Physics **156**, 124107 (2022).
- [45] J. Westermayr, S. Chaudhuri, A. Jeindl, O. T. Hofmann, and R. J. Maurer, Digital Discovery **1**, 463 (2022).
- [46] S. A. Ghasemi, A. Hofstetter, S. Saha, and S. Goedecker, Phys. Rev. B **92**, 045131 (2015).
- [47] T. W. Ko, J. A. Finkler, S. Goedecker, and J. Behler, Nature Communications **12**, 398 (2021).
- [48] C. G. Staacke, S. Wengert, C. Kunkel, G. Csányi, K. Reuter, and J. T. Margraf, Machine Learning: Science and Technology **3**, 015032 (2022).
- [49] Y. Shao, L. Andersson, L. Knijff, and C. Zhang, Electronic Structure **4**, 014012 (2022).
- [50] T. Dufils, L. Knijff, Y. Shao, and C. Zhang, ArXiv Prepr. ArXiv2303.15307 (2023).
- [51] A. Grisafi, D. M. Wilkins, G. Csányi, and M. Ceriotti, Phys. Rev. Lett. **120**, 036002 (2018).
- [52] F. Musil, A. Grisafi, A. P. Bartók, C. Ortner, G. Csányi, and M. Ceriotti, Chemical Reviews **121**, 9759 (2021).
- [53] V. L. Deringer, A. P. Bartók, N. Bernstein, D. M. Wilkins, M. Ceriotti, and G. Csányi, Chemical Reviews **121**, 10073 (2021).
- [54] A. P. Bartók, R. Kondor, and G. Csányi, Phys. Rev. B **87**, 184115 (2013).
- [55] A. Fabrizio, K. Briling, A. Grisafi, and C. Corminboeuf, CHIMIA International Journal for Chemistry **74**, 232 (2020).
- [56] A. Grisafi and M. Ceriotti, J. Chem. Phys. **151**, 204105 (2019).
- [57] A. Grisafi, J. Nigam, and M. Ceriotti, Chem. Sci. **12**, 2078 (2021).
- [58] M. J. Willatt, F. Musil, and M. Ceriotti, The Journal of Chemical Physics **150**, 154110 (2019).
- [59] T. Laino, F. Mohamed, A. Laio, and M. Parrinello, Journal of Chemical Theory and Computation **2**, 1370 (2006).
- [60] J. P. Perdew, K. Burke, and M. Ernzerhof, Phys. Rev. Lett. **77**, 3865 (1996).
- [61] O. Vahtras, J. Almlöf, and M. Feyereisen, Chemical Physics Letters **213**, 514 (1993).
- [62] K. R. Briling, A. Fabrizio, and C. Corminboeuf, The Journal of Chemical Physics **155**, 024107 (2021).
- [63] A. Bussy, O. Schütt, and J. Hutter, The Journal of Chemical Physics **158**, 164109 (2023).
- [64] M. J. Willatt, F. Musil, and M. Ceriotti, Phys. Chem. Chem. Phys. **20**, 29661 (2018).
- [65] See Supplemental Material at [*URL will be set by the Editor*], which contains: details about the dataset generation, a derivation of the finite-field extension of LODE, details about the ML parameters, a discussion about charge conservation, complementary results, an explicit calculation of the electronic polarization vector, a discussion about the calculation the differential capacitance.
- [66] S. Theodoridis and K. Koutroumbas, *Pattern Recognition, Fourth Edition* (Academic Press, 2009).
- [67] T. Dufils, G. Jeanmairet, B. Rotenberg, M. Sprik, and M. Salanne, Phys. Rev. Lett. **123**, 195501 (2019).
- [68] C. Zhang, T. Sayer, H. Hutter, and M. Sprik, Journal of Physics: Energy **2**, 032005 (2020).
- [69] A. Marin-Lafèche, M. Haelele, L. Scalfi, A. Coretti, T. Dufils, G. Jeanmairet, S. K. Reed, A. Serva, R. Berthin, C. Bacon, S. Bonella, B. Rotenberg, P. A. Madden, and M. Salanne, Journal of Open Source Software **5**, 2373 (2020).
- [70] T. Darden, D. York, and L. Pedersen, The Journal of Chemical Physics **98**, 10089 (1993).
- [71] A. K. Lautar, A. Hagopian, and J.-S. Filhol, Phys. Chem. Chem. Phys. **22**, 10569 (2020).
- [72] A. M. Lewis, P. Lazzaroni, and M. Rossi, The Journal of Chemical Physics **159**, 014103 (2023).
- [73] A. U. Chowdhury, N. Muralidharan, C. Daniel, R. Amin, and I. Belharouak, Journal of Power Sources **506**, 230173 (2021).